

Article

Excellent Room-Temperature Thermoelectricity of 2D GeP₃: Mexican-Hat-Shaped Band Dispersion and Ultralow Lattice Thermal Conductivity

Cong Wang^{1,2,†}, Zhiyuan Xu^{1,†}, Ke Xu² and Guoying Gao^{1,*}

¹ School of Physics, Huazhong University of Science and Technology, Wuhan 430074, China; phywangc@hbuas.edu.cn (C.W.); xzy6517@163.com (Z.X.)

² Hubei Key Laboratory of Low Dimensional Optoelectronic Materials and Devices, Hubei University of Arts and Science, Xiangyang 441053, China; xuke@hbuas.edu.cn

* Correspondence: guoying_gao@mail.hust.edu.cn

† These authors contributed equally to this work.

Abstract: Although some atomically thin 2D semiconductors have been found to possess good thermoelectric performance due to the quantum confinement effect, most of their behaviors occur at a higher temperature. Searching for promising thermoelectric materials at room temperature is meaningful and challenging. Inspired by the finding of moderate band gap and high carrier mobility in monolayer GeP₃, we investigated the thermoelectric properties by using semi-classical Boltzmann transport theory and first-principles calculations. The results show that the room-temperature lattice thermal conductivity of monolayer GeP₃ is only 0.43 Wm⁻¹K⁻¹ because of the low group velocity and the strong anharmonic phonon scattering resulting from the disordered phonon vibrations with out-of-plane and in-plane directions. Simultaneously, the Mexican-hat-shaped dispersion and the orbital degeneracy of the valence bands result in a large *p*-type power factor. Combining this superior power factor with the ultralow lattice thermal conductivity, a high *p*-type thermoelectric figure of merit of 3.33 is achieved with a moderate carrier concentration at 300 K. The present work highlights the potential applications of 2D GeP₃ as an excellent room-temperature thermoelectric material.

Keywords: thermoelectricity; power factor; lattice thermal conductivity; GeP₃ monolayer; first-principles; Boltzmann transport



Citation: Wang, C.; Xu, Z.; Xu, K.; Gao, G. Excellent Room-Temperature Thermoelectricity of 2D GeP₃: Mexican-Hat-Shaped Band Dispersion and Ultralow Lattice Thermal Conductivity. *Molecules* **2021**, *26*, 6376. <https://doi.org/10.3390/molecules26216376>

Academic Editor: Saulius Grigalevicius

Received: 16 September 2021

Accepted: 19 October 2021

Published: 21 October 2021

Publisher's Note: MDPI stays neutral with regard to jurisdictional claims in published maps and institutional affiliations.



Copyright: © 2021 by the authors. Licensee MDPI, Basel, Switzerland. This article is an open access article distributed under the terms and conditions of the Creative Commons Attribution (CC BY) license (<https://creativecommons.org/licenses/by/4.0/>).

1. Introduction

Thermoelectric (TE) materials, which could convert thermal energy into electric energy, have become more and more important due to their potential in resolving the global warming and the energy dilemma [1,2]. The efficiency of TE conversion is quantified by the TE figure of merit $ZT = S^2\sigma T/\kappa$. Here, T is the temperature, σ is the electrical conductivity, S is the Seebeck coefficient, and κ is the sum of electronic and phonon (lattice) thermal conductivity. These TE coefficients are connected by the carrier concentration and will lead to a maximum ZT value at a proper carrier concentration. In the past few years, numerous efforts have suggested that the TE performance of low-dimensional systems could be enhanced compared to their bulk counterparts because of the quantum confinement effect [3–5].

Graphene-like atomically thin 2D materials, such as germanene, black phosphorene, arsenene, silicene, and transition-metal dichalcogenides monolayers have attracted intense interest in thermoelectrics recently [6–11]. Some of them showed excellent TE performance at a moderate or higher temperature. As we all know, TE materials with higher ZT values at room temperature will make them commercially viable for the cooling and power generation field [12]. However, searching for room-temperature 2D high-performance TE materials is still challenging, because the relatively high lattice thermal conductivity at

room temperature hinders the increase of the ZT value. For example, the optimized ZT values at 300 K are only 0.01 for monolayer graphene, 0.16 for monolayer graphyne, 0.14 for monolayer WSe_2 [7,8]. Although the ZT value can reach 1.2 at 1200 K for p -type $CdPSe_3$, it is only 0.5 at room temperature [9]. Therefore, it is necessary to search for promising room-temperature TE materials.

Latterly, a new type of 2D monolayers MP_3 ($M = Ga, In, Ge, Sn$) received growing attention in view of their novel chemical and physical properties [13–21]. Their structures are associated with arsenic, which can be regarded as one M atom replacing every fourth atom in the arsenic layer and the rest replaced by phosphorus (P) atoms. Interestingly, when the thickness is equal to or greater than three layers, both SnP_3 and GeP_3 will become metals due to the correlation between lone-pair electrons of interlayer $Ge(Sn)$ and P atoms [13,14]. Importantly, all the MP_3 monolayers are predicted to be 2D semiconductors with high carrier mobilities and moderate energy gaps [13–16], and the biaxial compressive strain can lead to the transition of indirect-direct band gaps for both GeP_3 and SnP_3 [13–15]. In addition, both GeP_3 and SnP_3 monolayers have been predicted as promising candidates for future applications in Li-ion batteries and electrocatalysis [17,18]. Even so, there have been little research on the TE properties for 2D MP_3 [19–21]. We would like to explore and understand the electron and phonon transport properties of 2D GeP_3 belonging to an MP_3 family.

In this work, we demonstrate from the first-principles calculations that the GeP_3 monolayer obtains a superior p -type $S^2\sigma$ due to the Mexican-hat-shaped dispersion and the orbital degeneracy for the valence bands. Meanwhile, an ultralow lattice thermal conductivity is obtained and understood from the phonon spectrum, phonon group velocity, Grüneisen parameter, vibration modes of lattice, and three-phonon scattering phase space. The superior power factor and the ultralow lattice conductivity lead to a high p -type ZT value of 3.33 at 300 K, which indicates the potential of monolayer GeP_3 as a room-temperature TE material.

2. Computational Methods

Our calculations include three parts. Firstly, the structural optimization of the GeP_3 monolayer is achieved by the VASP code [22]. The generalized gradient approximation (GGA) in the Perdew–Burke–Ernzerhof (PBE) type is adopted for the exchange–correlation functional [23]. A 550 eV is set for the cutoff energy, and a $15 \times 15 \times 1$ q-grid is chosen in the Brillouin zone. We use the hybrid functional (HSE06) [24] to obtain the band structure and the electronic transport properties because the GGA usually underestimates the band gap.

Secondly, the electronic transport properties are computed by the Boltzmann transport theory within the relaxation time approximation in the BoltzTraP code [25]. The κ_e is conducted by the Wiedemann–Franz law $\kappa_e = L\sigma T$, here, $L = 2.44 \times 10^{-8} \text{ W}\Omega\text{K}^{-2}$ represents the Lorentz number [26]. The carrier relaxation time τ is estimated by the deformation potential theory, which has been extensively applied for 2D systems [6,27,28]. The calculated electron (hole) relaxation time at room temperature is $1.9 (6.2) \times 10^{-13} \text{ s}$, which is close to the results obtained by Zeng et al. [29].

Thirdly, the thermal transport properties are obtained via solving the phonon Boltzmann transport equation with ShengBTE [30]. A $4 \times 4 \times 1$ supercell with $7 \times 7 \times 1$ k -mesh is chosen to acquire the second-order and third-order interatomic force constants (IFCs). The cutoff of interaction is up to the sixth nearest neighbors for the anharmonic IFCs. The interlayer separation of bulk is used as the thickness of the monolayer to calculate the lattice thermal conductivity, which has been used in other 2D monolayers [31,32]. It is worth noting that the present computational approaches of transport properties have been reviewed recently by Kozinsky and Singh [33].

3. Results and Discussion

The crystal structure of the GeP_3 monolayer is plotted in Figure 1a,b. The optimized lattice constant $a = b = 6.96 \text{ \AA}$ is closed to the earlier theoretical values [13,17,18]. We first

calculate the electronic band structure and the density of states (DOS) within HSE06. It is distinctly seen in Figure 1c that the GeP₃ monolayer is an indirect band gap (0.53 eV) semiconductor, which is consistent with the value of 0.55 eV reported by Jing et al [13]. The calculated total and atomic orbit-resolved DOS (Figure 1d) reveal that both conduction bands and valence bands derive from the hybridized P and Ge *p* orbitals. The uppermost valence bands emerge so-called “Mexican-hat-shaped” dispersion, which can greatly enhance the TE properties [34,35]. As can be seen from Figure 1c, the “Mexican-hat-shaped” dispersion on the top of valence bands show heavy and light bands simultaneously. The heavy bands along the *M-K* direction are very flat, which will lead to a large DOS effective mass and thus, a large Seebeck coefficient. Meanwhile, the light bands with distinct dispersion along *M-Γ* and *K-Γ* directions will result in high electrical conductivity. Moreover, the two separated bands are degenerate at the *K* point on the top of the valence bands. Such degenerate band structure feature is considered to take great effect on electronic transport and will give rise to a high density-of-state effective mass and in turn a large Seebeck coefficient [36,37].

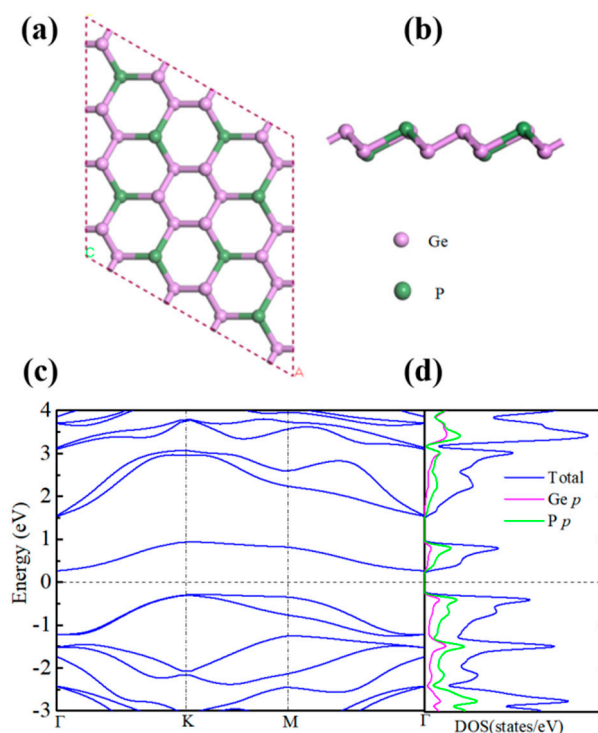


Figure 1. The top (a) and side (b) views of the crystal structure and the band structure (c) and atomic orbit-resolved density of states (d) for monolayer GeP₃. The pink and green balls represent the Ge and P atoms, respectively.

On the basis of the obtained band structure of the GeP₃ monolayer, we further computed the electronic transport properties including the S , σ , PF , and κ_e . We simulate the doping by the rigid band approximation. The obtained σ and S with the change of carrier concentration n at three different temperatures are shown in Figure 2a–d. As can be seen, the Seebeck coefficient of *p*-type doping is larger than that of *n*-type doping due to the flat valence bands along the *M-K* direction and the band degeneracy at the *K* point. With assured carrier concentration, the Seebeck coefficient increases with the increase of temperature. Besides, the *p*-type doping σ is much larger than that of *n*-type doping because of the strong dispersion along the *M-Γ* and *K-Γ* directions. It is natural the maximum power factor can be achieved in *p*-type because a larger Seebeck coefficient and higher electrical conductivity are obtained in *p*-type simultaneously. By comparing the S and σ values of the *p*-type and *n*-type for monolayer GeP₃, it is found that the “Mexican-hat-shaped”

dispersion for valence band structure can not only significantly increase the S by the flat band, but also avoid the poor performance of the σ . Figure 2e, f shows the power factor $S^2\sigma$. It can be seen that the p -type $S^2\sigma$ is much larger than that of the n -type one, which implies that greater TE performance could be achieved by the p -type doping. Typically, the obtained room-temperature p -type $S^2\sigma$ is about $0.0245 \text{ Wm}^{-1}\text{K}^{-2}$ for monolayer GeP_3 , which is even larger than the well-known TE material Bi_2Te_3 ($0.003 \text{ Wm}^{-1}\text{K}^{-2}$) [38]. In addition, the plotted electronic thermal conductivity κ_e (Figure 2g,h) indicates that the changes of σ and κ_e with temperature and carrier concentration are uniform due to their correlation according to the Wiedemann–Franz law [26].

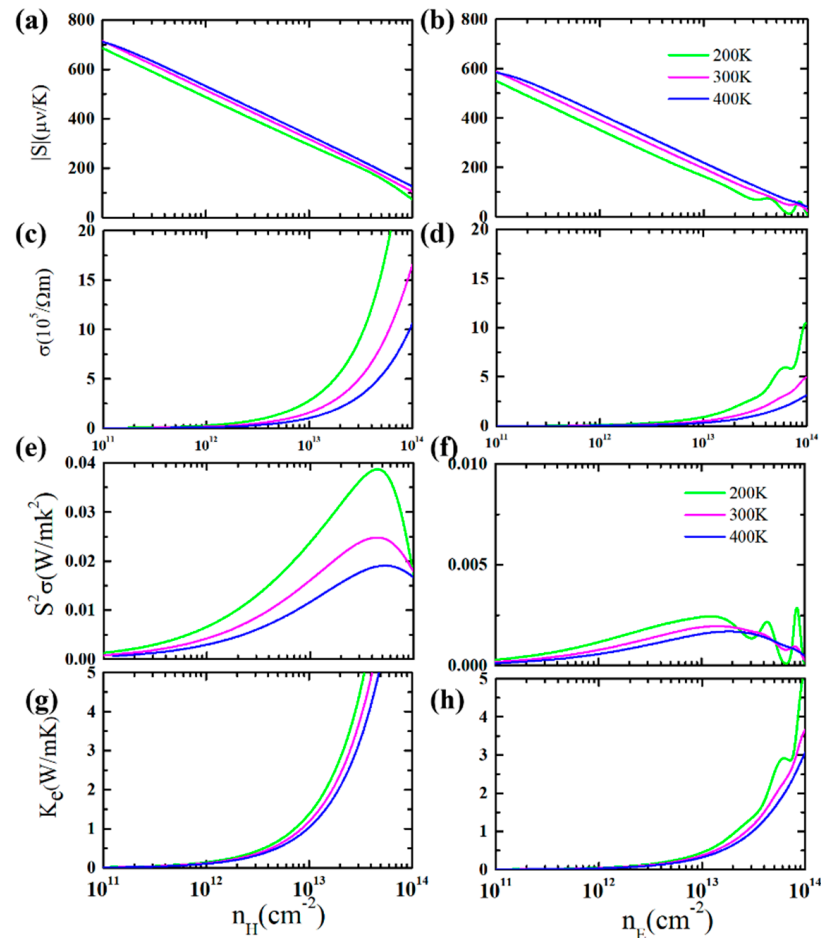


Figure 2. The absolute value of Seebeck coefficient (a,b), the electrical conductivity (c,d), the power factor (e,f), and the electronic thermal conductivity (g,h) with the change of carrier concentration and temperature for monolayer GeP_3 . The left (right) part represents the p -type (n -type) doping.

After attaining the electronic transport properties of the GeP_3 monolayer, we now examine the phonon transport property. The obtained phonon band structure and phonon density of states of GeP_3 monolayer are presented in Figure 3a. No imaginary phonon frequency appears which implies the stability of monolayer GeP_3 . The lowest three phonon modes at the Γ point are acoustic phonon branches, i.e., the in-plane transverse acoustic branch (TA), the z -direction acoustic mode (ZA), and the in-plane longitudinal acoustic branch (LA). The maximum frequency of acoustic branches is only 1.81 THz, which is comparable or lower than those of admirable TE materials, such as PbTe and SnSe [39], indicating a smaller phonon group velocity in monolayer GeP_3 . In addition, the flat phonon dispersion characteristics of acoustic branches closed to the Γ point is also a key to obtaining a small phonon group velocity and a low lattice thermal conductivity. As expected, the group velocities that could be computed by $\partial\omega/\partial k$ are 1.70, 1.27 and 1.63 kms^{-1} for

the LA, ZA and TA branches at the Γ point, respectively, which are smaller than those of PbTe, SnSe [39], and SnTe [10]. Meanwhile, the low-frequency optical branches are overlapped and mixed with the acoustic modes, resulting in strong interactions and large three-phonon processes, which will have a great influence on the κ_l of monolayer GeP₃. The calculated total and partial phonon DOS show that the low-frequency optical branches and the acoustic modes are derived from the vibrations of the Ge and P atom while the P atom forms the high-frequency optical modes. So, the thermal carry through the Ge–P bond is the major heat transfer means in the GeP₃ monolayer. Due to the flat phonon dispersion closed to the Γ point for acoustic branches, the PhDOS is truly sharp, and consequently, a low κ_l could be anticipated.

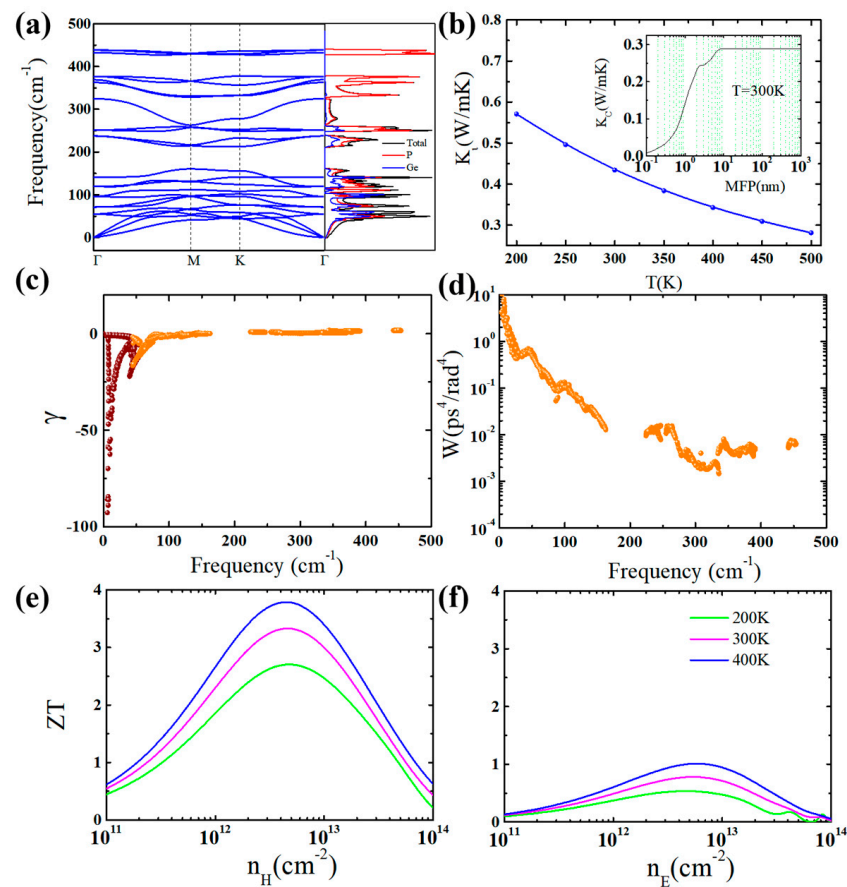


Figure 3. The phonon dispersion (a), the temperature-dependent lattice thermal conductivity (b), the frequency-dependent Grüneisen parameter γ (c) and three-phonon scattering phase space W (d) at 300 K, and the p -type (e) and n -type (f) figure of merit ZT with the change of carrier concentration and temperature for monolayer GeP₃. The inset in (b) shows the cumulative lattice thermal conductivity as a function of phonon mean-free-path (MFP) at 300 K.

The κ_l which is computed by solving the phonon Boltzmann transport equation performed in ShengBTE [30] can be expressed as

$$\kappa_{L,\alpha\beta} = \sum_{qs} C_V(qs) v_g^\alpha(qs) v_g^\beta(qs) \tau_{qs} \quad (1)$$

where q , s , C_V , v_g , and τ represent the wave vector, the dispersion branch, the phonon mode volumetric specific heat, the group velocity, and the phonon lifetime, respectively. The calculated κ_l for monolayer GeP₃ as a function of temperature T is plotted in Figure 3b. It can be seen that the κ_l for the GeP₃ monolayer is fairly low, especially at a high temperature. Typically, the κ_l for the GeP₃ monolayer is only $0.43 \text{ Wm}^{-1}\text{K}^{-1}$ at 300 K, which is much lower

than those of good TE materials of SnSe ($0.62 \text{ Wm}^{-1}\text{K}^{-1}$) and PbTe ($2.30 \text{ Wm}^{-1}\text{K}^{-1}$) [39], as well as 2D CdPSe₃ ($1.25 \text{ Wm}^{-1}\text{K}^{-1}$) [9]. Such low κ_l means that monolayer GeP₃ could be a favorable room-temperature TE material. Note that, in our calculations based on the phonon Boltzmann transport equation (ShengBTE code) [30], the phonon-phonon, the isotope and the boundary scatterings are included, but the carrier-phonon scattering is not considered. So, the lattice thermal conductivity κ_l is independent of the carrier concentration n . In Figure 4, we present a comparison of the calculated κ_l and κ_e . One can see that the characteristics of $(\kappa_e + \kappa_l) \sim n$ is similar to that of $\kappa_e \sim n$. The κ_l is higher than the κ_e at the low n , but it is opposite at the high n .

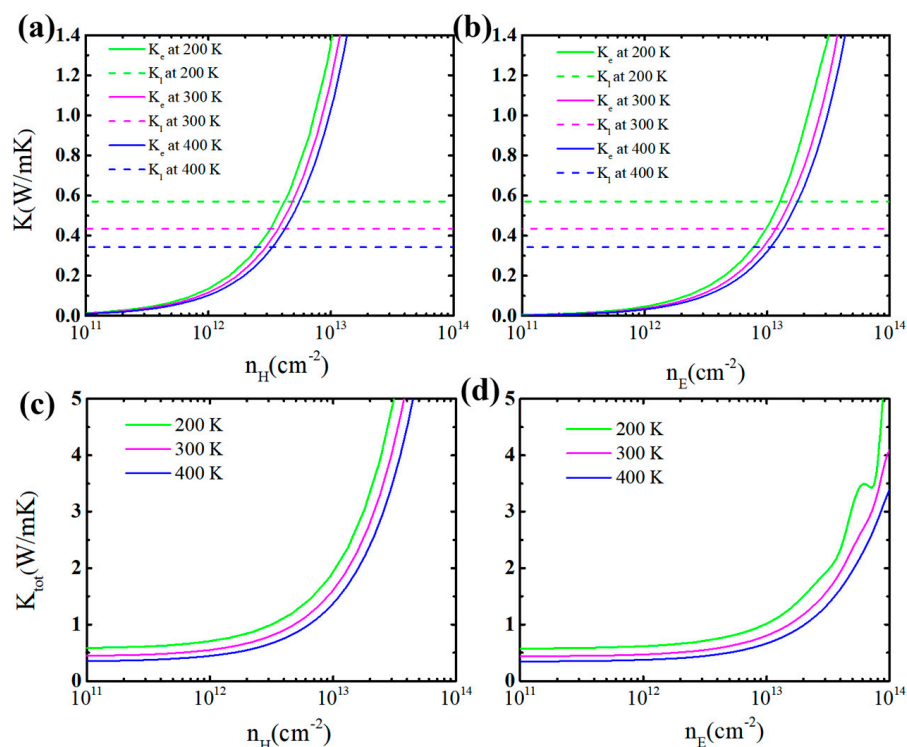


Figure 4. The electron (κ_e) and phonon (κ_l) thermal conductivity (a,b) as well as the total (κ_{tot}) thermal conductivity (c,d) with the change of carrier concentration and temperature for monolayer GeP₃. The left (right) part represents the *p*-type (*n*-type) doping.

To get more perception for the phonon thermal transport properties, we calculate the three phonon scattering phase space W and Grüneisen parameter γ for monolayer GeP₃, as plotted in Figure 3c,d. The γ could qualitatively characterize the anharmonic phonon scattering, and the W could give the comprehension of the number of available channels for anharmonic phonon scattering. Usually, larger $|\gamma|$ means strong anharmonic phonon scattering and thus leads to a low κ_l . The calculated average value of the Grüneisen parameter $|\gamma|$ for acoustic branches is 9.6, which is high and indicates the strong anharmonicity and thus a low κ_l can be obtained for monolayer GeP₃. In addition, it is found that the large Grüneisen parameter and three phonon phase space mainly exist in the low-frequency region, especially for the acoustic branches, which reveals that the acoustic branches contribute most to the total lattice thermal conductivity.

Besides, we study the phonon vibration modes in terms of the computed 2nd IFCs. We show in Figure 5 some typical vibration modes of monolayer GeP₃ at Γ point. The phonon modes presented in Figure 5a–c are the vibration of three acoustic modes (LA, TA and ZA, respectively). The results show that the vibration directions of these branches are firmly along the out-of-plane (ZA) or the in-plane (LA and TA). Figure 5d is the vibration type of the lowest optical mode. In this mode, the Ge atoms are fixed, some P atoms vibrate out-of-plane, while other P atoms move in-plane in different directions. Similar phonon

vibration modes could also be observed in higher-frequency optical branches (Figure 5e,f). These optical modes are effortlessly thermally activated at 300 K and seriously hinder thermal transport as a result of phonon-phonon scattering, and thus, a low κ_l is gained for monolayer GeP₃.

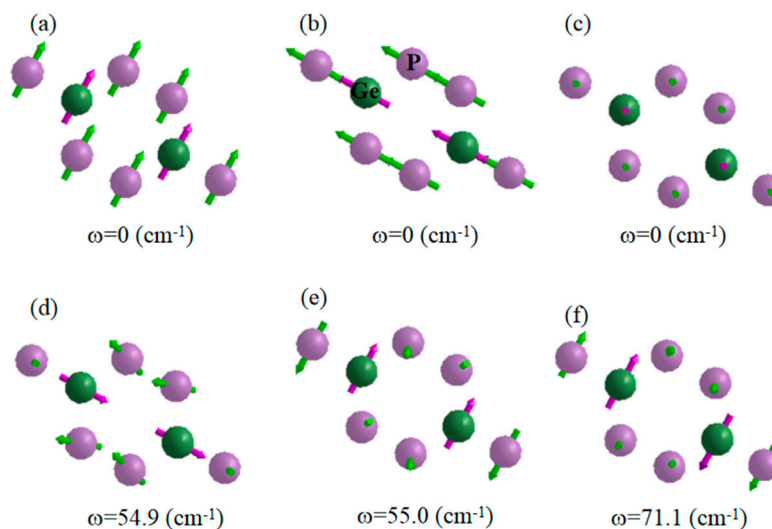


Figure 5. The typical vibrational modes of the acoustic phonon branches (LA (a), TA (b) and ZA (c)) as well as three low-frequency optical phonon branches (d–f) for monolayer GeP₃ at the Γ point. The arrows denote the atomic displacement directions at 300 K.

Nanostructure is one of the important ways to enhance ZT value by hindering phonon transport [3–5]. The phonon boundary scattering would greatly depress the κ_l as long as the length of the nanostructure is as short as the phonon mean free path (MFP). Therefore, the discussion on phonon MFP is necessary to study the size effect and also significant to design nano TE devices. The calculated cumulative lattice thermal conductivity (κ_C) in regard to MFP at 300 K for monolayer GeP₃ is shown in the inset of Figure 3b. The calculated κ_C keeps increasing as the increase of MFP till the thermodynamic limit is reached. The critical value of MFP (l_0) to the maximum lattice thermal conductivity at 300 K is only 8.2 nm. In general, nanostructures with l_0 short than 10 nm is favorable for their TE performance. By comparing with other TE materials, monolayer GeP₃ shows a fairly low l_0 value. Thus, the intrinsically short MFP for monolayer GeP₃ hinders the potential for further decrease of κ_l . In other words, the effect of size on κ_l for monolayer GeP₃ is not so significant.

Finally, according to the above calculated thermal transport coefficients, we computed the ZT value with the change of temperature and carrier concentration. Note that, the present ZT is an estimation based on the relaxation time approximation, because the carrier relaxation time is complex, and it is approximated as a constant in the present calculations by the BoltzTraP code [25] based on the Boltzmann transport theory. As shown in Figure 3e,f, the optimal ZT value increases with the increasing temperature. The p -type has high ZT value than the n -type because of the large power factor of p -type than n -type. For the p -type doping at 300 K, the optimal ZT value for monolayer GeP₃ is as large as 3.33 with a large Seebeck coefficient of 400 $\mu\text{V}/\text{K}$ at the hole concentration of $5.07 \times 10^{12} \text{ cm}^{-2}$, while the value is only 0.78 for the n -type doping. Therefore, monolayer GeP₃ is an excellent p -type room-temperature TE material due to the high-power factor and the low thermal conductivity. The optimal p -type ZT value of 3.33 at 300 K is higher than most of 2D semiconductors, such as p -type CdPSe₃ (0.5 at 300 K) [9], p -type InP₃ (2.06 along the armchair direction at 300 K) [19], and n -type α -In₂Se₃ (2.18 at 300 K) [40], etc.

4. Conclusions

In summary, thanks to the recent finding of monolayer GeP₃ with high carrier mobility and a moderate energy gap, we perform the first principles to explore the electron and phonon transport properties for monolayer GeP₃. The Mexican-hat-shaped dispersion and the band degeneracy of valence bands result in a high *p*-type power factor. The low frequency of acoustic branches, low phonon group velocity, large Grüneisen parameter and large three-phonon scattering phase space result in an ultralow lattice thermal conductivity of 0.43 Wm⁻¹K⁻¹ at 300 K. Therefore, a high *p*-type *ZT* value of 3.33 is achieved at 300 K, which is higher than most of the 2D semiconductors, making monolayer GeP₃ an excellent room TE material.

Author Contributions: Formal analysis, K.X.; Investigation, C.W.; Methodology, Z.X.; Supervision, G.G.; Writing—original draft, C.W.; Writing—review & editing, G.G. All authors have read and agreed to the published version of the manuscript.

Funding: This work was funded by the National Natural Science Foundation of China (grant No. 12174127).

Institutional Review Board Statement: Not applicable.

Informed Consent Statement: Not applicable.

Data Availability Statement: Not applicable.

Conflicts of Interest: The authors declare no conflict of interest.

Sample Availability: Samples of the compounds are not available from the authors.

References

1. Bell, L.E. Cooling, heating, generating power, and recovering waste heat with thermoelectric systems. *Science* **2008**, *321*, 1457–1461. [[CrossRef](#)]
2. Mao, J.; Liu, Z.; Zhou, J.; Zhu, H.; Zhang, Q.; Chen, G.; Ren, Z. Advances in thermoelectrics. *Adv. Phys.* **2018**, *67*, 69–147. [[CrossRef](#)]
3. Dong, Z.; Xu, H.; Liang, F.; Luo, C.; Wang, C.; Cao, Z.-Y.; Chen, X.-J.; Zhang, J.; Wu, X. Raman characterization on two-dimensional materials-based thermoelectricity. *Molecules* **2019**, *24*, 88. [[CrossRef](#)] [[PubMed](#)]
4. Hung, N.T.; Nugraha, A.R.T.; Yang, T.; Saito, R. Confinement effect in thermoelectric properties of two-dimensional materials. *MRS Adv.* **2020**, *5*, 469–479. [[CrossRef](#)]
5. Hung, N.T.; Saito, R. The origin of quantum effects in low-dimensional thermoelectric materials. *Adv. Quantum Technol.* **2021**, *4*, 2000115. [[CrossRef](#)]
6. Wang, C.; Zheng, C.; Gao, G. Bulk and monolayer ZrS₃ as promising anisotropic thermoelectric materials: A comparative study. *J. Phys. Chem. C* **2020**, *124*, 6536–6543. [[CrossRef](#)]
7. Wang, X.-M.; Mo, D.-C.; Lu, S.-S. On the thermoelectric transport properties of graphyne by the first-principles method. *J. Chem. Phys.* **2013**, *138*, 204704. [[CrossRef](#)]
8. Kumar, S.; Schwingschlogl, U. Thermoelectric response of bulk and monolayer MoSe₂ and WSe₂. *Chem. Mater.* **2015**, *27*, 1278–1284. [[CrossRef](#)]
9. Yun, W.S.; Lee, J.D. Single-layer CdPSe₃: A promising thermoelectric material persisting in high temperatures. *Appl. Phys. Lett.* **2019**, *115*, 193105. [[CrossRef](#)]
10. Li, Y.; Wu, M.N.; Ding, T.; Ma, K.; Liu, F.S.; Ao, W.Q.; Li, J.Q. Promising thermoelectric properties and anisotropic electrical and thermal transport of monolayer SnTe. *Appl. Phys. Lett.* **2019**, *114*, 083901. [[CrossRef](#)]
11. Patel, A.; Singh, D.; Sonvane, Y.; Thakor, P.B.; Ahuja, R. High thermoelectric performance in two-dimensional Janus monolayer material WS-X (X= Se and Te). *ACS Appl. Mater. Interfaces* **2020**, *12*, 46212–46219. [[CrossRef](#)] [[PubMed](#)]
12. Hu, L.; Wu, H.; Zhu, T.; Fu, C.; He, J.; Ying, P.; Zhao, X. Tuning multiscale microstructures to enhance thermoelectric performance of n-type Bismuth-Telluride-based solid solutions. *Adv. Energy Mater.* **2015**, *5*, 1500411. [[CrossRef](#)]
13. Jing, Y.; Ma, Y.; Li, Y.; Heine, T. GeP₃: A small indirect band gap 2D crystal with high carrier mobility and strong interlayer quantum confinement. *Nano Lett.* **2017**, *17*, 1833–1838. [[CrossRef](#)]
14. Gong, P.-L.; Zhang, F.; Huang, L.-F.; Zhang, H.; Li, L.; Xiao, R.-C.; Deng, B.; Pan, H.; Shi, X.-Q. Multifunctional two-dimensional semiconductors SnP₃: Universal mechanism of layer-dependent electronic phase transition. *J. Phys. Condens. Matter* **2018**, *30*, 475702. [[CrossRef](#)]
15. Sun, S.; Meng, F.; Wang, H.; Wang, H.; Ni, Y. Novel two-dimensional semiconductor SnP₃: High stability, tunable bandgaps and high carrier mobility explored using first-principles calculations. *J. Mater. Chem. A* **2018**, *6*, 11890–11897. [[CrossRef](#)]
16. Miao, N.; Xu, B.; Bristowe, N.C.; Zhou, J.; Sun, Z. Tunable magnetism and extraordinary sunlight absorbance in indium triphosphide monolayer. *J. Am. Chem. Soc.* **2017**, *139*, 11125–11131. [[CrossRef](#)]

17. Zhang, C.; Jiao, Y.; He, T.; Ma, F.; Kou, L.; Liao, T.; Bottle, S.; Du, A. Two-dimensional GeP₃ as a high capacity electrode material for Li-ion batteries. *Phys. Chem. Chem. Phys.* **2017**, *19*, 25886–25890. [[CrossRef](#)] [[PubMed](#)]
18. Wu, H.-H.; Huang, H.; Zhong, J.; Yu, S.; Zhang, Q.; Zeng, X.C. Monolayer triphosphates MP₃(M=Sn, Ge) with excellent basal catalytic activity for hydrogen evolution reaction. *Nanoscale* **2019**, *11*, 12210–12219. [[CrossRef](#)]
19. Ouyang, T.; Jiang, E.; Tang, C.; Li, J.; He, C.; Zhong, J. Thermal and thermoelectric properties of monolayer indium triphosphide (InP₃): A first-principles study. *J. Mater. Chem. A* **2018**, *6*, 21532–21541. [[CrossRef](#)]
20. Sun, Z.; Yuan, K.; Chang, Z.; Bi, S.; Zhang, X.; Tang, D. Ultra-low thermal conductivity and high thermoelectric performance of two-dimensional triphosphides (InP₃, GaP₃, SbP₃ and SnP₃): A comprehensive first-principles study. *Nanoscale* **2020**, *12*, 3330–3342. [[CrossRef](#)] [[PubMed](#)]
21. Zhu, X.-L.; Liu, P.-F.; Zhang, J.; Zhang, P.; Zhou, W.-X.; Xie, G.; Wang, B.-T. Monolayer SnP₃: An excellent p-type thermoelectric material. *Nanoscale* **2019**, *11*, 19923–19932. [[CrossRef](#)]
22. Kresse, G.; Furthmüller, J. Efficient iterative schemes for ab initio total-energy calculations using a plane-wave basis set. *Phys. Rev. B* **1996**, *54*, 11169. [[CrossRef](#)]
23. Perdew, J.P.; Burke, K.; Ernzerhof, M. Generalized gradient approximation made simple. *Phys. Rev. Lett.* **1997**, *78*, 1396. [[CrossRef](#)]
24. Heyd, J.; Scuseria, G.E.; Ernzerhof, M. Hybrid functionals based on a screened Coulomb potential. *J. Chem. Phys.* **2003**, *118*, 8207–8215. [[CrossRef](#)]
25. Madsen, G.K.H.; Singh, D.J. BoltzTraP. A code for calculating band-structure dependent quantities. *Comput. Phys. Commun.* **2006**, *175*, 67–71. [[CrossRef](#)]
26. Jonson, M.; Mahan, G.D. Mott's formula for the thermopower and the Wiedemann-Franz law. *Phys. Rev. B* **1980**, *21*, 4223. [[CrossRef](#)]
27. Zhang, W.; Huang, Z.; Zhang, W.; Li, Y. Two-dimensional semiconductors with possible high room temperature mobility. *Nano Res.* **2014**, *7*, 1731–1737. [[CrossRef](#)]
28. Wang, C.; Wei, S.; Gao, G. Theoretical investigation of metal-shrouded Ti₂O monolayers: Pudding-mold-type band structure and thermoelectric performance. *ACS Appl. Nano Mater.* **2019**, *2*, 4061–4066. [[CrossRef](#)]
29. Zeng, B.; Long, M.; Zhang, X.; Dong, Y.; Li, M.; Yi, Y.; Duan, H. Strain engineering on electronic structure and carrier mobility in monolayer GeP₃. *J. Phys. D Appl. Phys.* **2018**, *51*, 235302. [[CrossRef](#)]
30. Li, W.; Carrete, J.; Katcho, N.A.; Mingo, N. ShengBTE: A solver of the Boltzmann transport equation for phonons. *Comput. Phys. Commun.* **2014**, *185*, 1747–1758. [[CrossRef](#)]
31. Zhang, J.; Liu, X.; Wen, Y.; Shi, L.; Chen, R.; Liu, H.; Shan, B. Titanium trisulfide monolayer as a potential thermoelectric material: A first-principles-based Boltzmann transport study. *ACS Appl. Mater. Interfaces* **2017**, *9*, 2509–2515. [[CrossRef](#)] [[PubMed](#)]
32. Rashid, Z.; Nissimogoudar, A.S.; Li, W. Phonon transport and thermoelectric properties of semiconducting Bi₂Te₂X (X=S, Se, Te) monolayers. *Phys. Chem. Chem. Phys.* **2019**, *21*, 5679–5688. [[CrossRef](#)]
33. Kozinsky, B.; Singh, D.J. Thermoelectrics by Computational Design: Progress and Opportunities. *Ann. Rev. Mater. Res.* **2021**, *51*, 565–590. [[CrossRef](#)]
34. Wickramaratne, D.; Zahid, F.; Lake, R.K. Electronic and thermoelectric properties of van der Waals materials with ring-shaped valence bands. *J. Appl. Phys.* **2015**, *118*, 075101. [[CrossRef](#)]
35. Çınar, M.N.; Sargun, G.Ö.; Sevim, K.; Özdamar, B.; Kurt, G.; Sevinçli, H. Ballistic thermoelectric transport properties of two-dimensional group III-VI monolayers. *Phys. Rev. B* **2021**, *103*, 165422. [[CrossRef](#)]
36. Zhu, H.; He, R.; Mao, J.; Zhu, Q.; Li, C.; Sun, J.; Ren, W.; Wang, Y.; Liu, Z.; Tang, Z.; et al. Discovery of ZrCoBi based half Heuslers with high thermoelectric conversion efficiency. *Nat. Commun.* **2018**, *9*, 2497. [[CrossRef](#)]
37. Ding, G.; Wang, C.; Gao, G.; Yao, K.; Dun, C.; Feng, C.; Li, D.; Zhang, G. Engineering of charge carriers via a two-dimensional heterostructure to enhance the thermoelectric figure of merit. *Nanoscale* **2018**, *10*, 7077–7084. [[CrossRef](#)]
38. Cheng, L.; Liu, H.J.; Zhang, J.; Wei, J.; Liang, J.H.; Shi, J.; Tang, X.F. Effects of van der Waals interactions and quasiparticle corrections on the electronic and transport properties of Bi₂Te₃. *Phys. Rev. B* **2014**, *90*, 085118. [[CrossRef](#)]
39. Xiao, Y.; Chang, C.; Pei, Y.; Wu, D.; Peng, K.; Zhou, X.; Gong, S.; He, J.; Zhang, Y.; Zeng, Z.; et al. Origin of low thermal conductivity in SnSe. *Phys. Rev. B* **2016**, *94*, 125203. [[CrossRef](#)]
40. Nian, T.; Wang, Z.; Dong, B. Thermoelectric properties of α-In₂Se₃ monolayer. *Appl. Phys. Lett.* **2021**, *118*, 033103. [[CrossRef](#)]